KSCE Journal of Civil Engineering (2019) 23(4):1548-1559

DOI 10.1007/s12205-019-0375-9

*Geotechnical Engineering*

pISSN 1226-7988, eISSN 1976-3808
www.springer.com/12205

# Centrifugal Model Test on the Failure Mechanism of Barrier Dam Overtopping

**Tianlong Zhao*, Shengshui Chen**, Changjing Fu***, and Qiming Zhong******

Received February 22, 2018/Revised August 15, 2018/Accepted November 7, 2018/Published Online January 18, 2019

## Abstract

In order to study the failure mechanism of barrier dam overtopping, centrifugal model tests of dam failure were conducted in this research. A calculation method of rectangular weir flow in the centrifugal field was derived. The process and mechanism of barrier dam overtopping were intensively analyzed. They were further verified by the breach flow curve and the development curve of the breach top width acquired from model tests. Results showed that the barrier dam breach developed during the entire process of overtopping in the width direction. The development of the barrier dam breach in the depth direction, however, ceased at an earlier time on account of the large particles accumulated in the downstream slope. Moreover, coarsening in the downstream slope could be clearly observed in the last stage of overtopping. Thus, it was concluded that the bottom part of the barrier dam could survive after dam breaching and that a full dam failure is relatively rare for a barrier dam. Furthermore, the size of the remaining breach would be less than that of a homogeneous earth dam under the same conditions.

Keywords: *barrier dam, overtopping failure, soil erosion, failure mechanism, centrifugal model test*

## 1. Introduction

A barrier dam is a type of natural rock-filled dam that is widely found throughout the world. The material composition and structure characteristics of a barrier dam are different from those of a general artificial dam because of the barrier dam's special formation. These dam types are extremely prone to breaking, and most of them will eventually disintegrate (Kuang 1993; Yan *et al*., 2009; Schuster *et al*., 1986; Mizuyama *et al*., 2008; Wan *et al*., 2004). Barrier dam life expectancy statistics are presented in Fig. 1. Once a dam breaks down, it can easily cause the severe hazard of a flood. Thus, it is necessary to study the dam break process and failure mechanism of the barrier dam. The findings can be highly significant to the development of a barrier dam break emergency plan, including emergency rescue operations.

The physical model test is a common and indispensable technique in the study of the dam failure mechanism (Li *et al*., 2009). Experimental research on an artificial-dam break can be traced to the middle of the 19$^{th}$ century. Numerous experimental studies on the process and mechanism of the artificial dam (homogeneous earth dam and core dam) have been conducted, such as the National Dam Safety Program (NDSP) conducted by the US Federal Emergency Management Agency (FEMA; Corns 2010); the CADAM Project, a concerted-action project funded under the European Commission (EC) FP4 Program (Morris 2000); the 2001 IMPACT project; and the 2004 FLOODsite Project, another EC-funded integrated project (Morris *et al*., 2005; Bruijn *et al*., 2009).

Experimental studies on barrier dam failures have been undertaken much more recently and with far less depth than those of artificial dam failures. As the number of barrier dams has increased in recent years, a series of barrier-dam failure model tests based on artificial-dam erosion model were performed. Research institutions that conducted these tests included the Civil Engineering Research Institute of Japan, the Chinese Academy of Sciences, the Nanjing Hydraulic Research Institute, and others. Several important achievements were hence made that elucidated barrier-dam break factors (Davies *et al*., 2007; Jiang, 2007; Wang *et al*., 2008; Gregoretti *et al*., 2010; Davies 2002; Zhao *et al*., 2016).

In actuality, however, few complete records exist of barrier-dam breaching processes. The small amount of research data that exists is predominantly from interviews and non-quantitative observations by witnesses (Becker *et al*., 2007). By comparison, model tests make it easier to obtain test data during the dam failure process. However, owing to the difficulty of model testing of a prototype dam, research to date on the barrier-dam failure mechanism has mainly focused small-scale model tests (Davies *et al*., 2007). The stress levels of models under a small scale are much different from those of the prototypical models, and it is

*Associate Professor, College of River and Ocean Engineering, Chongqing Jiaotong University, Chongqing 400060, China (E-mail: 990201500037@cqjtu.edu.cn)
**Professor, Dept. of Geotechnical Engineering, Nanjing Hydraulic Research Institute, Nanjing 210029, China (E-mail: sschen@nhri.cn)
***Associate Professor, College of River and Ocean Engineering, Chongqing Jiaotong University, Chongqing 400069, China (Corresponding Author, E-mail: 546684412@qq.com)
****Professor, Dept. of Geotechnical Engineering, Nanjing Hydraulic Research Institute, Nanjing 210029, China (E-mail: qmzhong@nhri.cn)

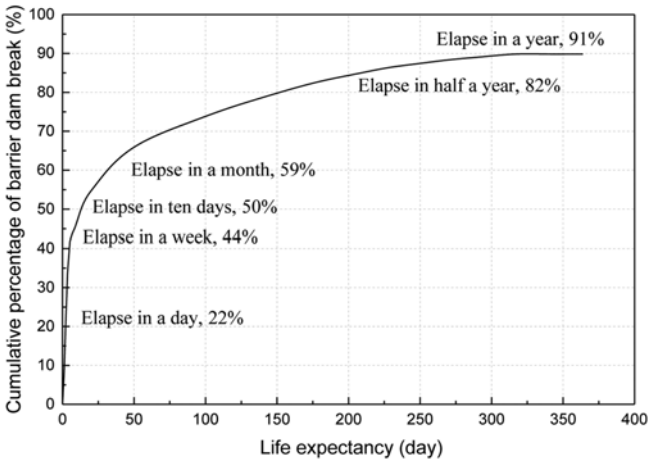


Fig. 1. Life Expectancy Statistics of Barrier Dam

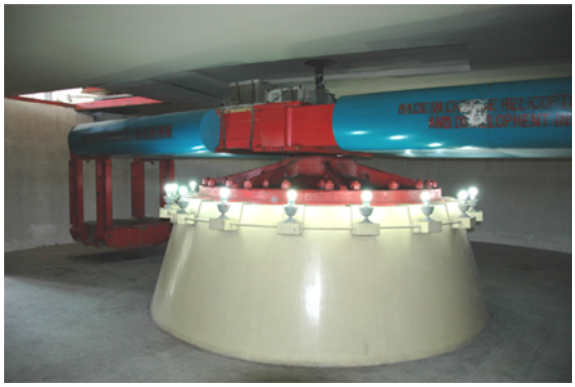

Fig. 2. The Geotechnical Centrifuge

thus difficult to reproduce a real dam break process of a barrier dam. The geotechnical centrifuge acceleration can be adjusted to accurately simulate the prototype stress field, which can reveal the failure mechanism and process of hydraulic structures constructed from soil and stone material. This test method can therefore be applied to the failure mechanism study of a barrier dam.

In the present work, the barrier-dam failure mechanism due to overtopping is the main focus. Based on the gradation curve of the Tangjiashan landslide dam—a landslide dam that was created at Tangjiashan during the 2008 Wenchuan earthquake of China's Southwest Sichuan Province—the centrifugal model test of barrier dam overtopping was recently performed. In this article, the process and mechanism of barrier dam overtopping are addressed, and the rules of breach development in horizontal and vertical directions, as well as the headcut erosion mechanism on a downstream slope, are revealed.

## 2. Experimental Apparatus and Methods

### 2.1 Experimental System of the Dam Break

Based on the centrifugal model test system of the Nanjing Hydraulic Research Institute (NHRI), model tests of barrier-dam overtopping were conducted. The dam-break test system consisted of a geotechnical centrifuge, an automatic flow control system, a special test box, and a data and image acquisition system.

#### 2.1.1 Geotechnical Centrifuge

The main equipment was a 400 gt large geotechnical centrifuge, as shown in Fig. 2. The maximum rotating radius of the centrifuge was 5.5 m, and the effective radius was 5.0 m. The maximum acceleration of the centrifuge was 200 g, and the maximum payload was 2 t.

#### 2.1.2 Water Supply

During the dam-break model testing, the model upstream was required to continually supply water until the end of the dam break. The automatic flow control system of the dam-break test system met the requirement of the water supply under high acceleration conditions. Through the sidewall outlets of the water-ring, water could be injected into the model test box smoothly under the effect of centrifugal force, and the smooth transition of break flow between normal and high gravity was achieved, as shown in Fig. 3.

#### 2.1.3 Test Box

The internal effective size of the test box was 1.2 × 0.4 × 0.8 m. The material of one side of the box was comprised of high transparent poly PMMA (methyl methacrylate). The other sides of the model box were comprised of 6061T6 high-strength aluminum alloy plates. The plates were fixed by bolts, and the jointing area between the panels was sealed with a rubber seal

(a) (b) (c)

Fig. 3. Water Supply System: (a) Water Tank (b) Water-ring (c) Outlet of the Water-ring

Fig. 4. The Test Box


Fig. 5. Layout of the Pore Pressure Measurement

strip to ensure that the tank did not leak during the test. The model test box is shown in Fig. 4.

The breach flow discharge is an important parameter for studying the failure mechanism of barrier dam overtopping, and it is necessary to accurately measure this parameter (Lobovsky *et al*., 2013). In the past, the flow meter was usually placed on the drainage outlet of the model box to monitor the export flow during the test. However, because the diameter of the circular outlet was too large, the tube could not be filled with water. In addition, the drainage water always carried a large amount of fine-particle sand, which could easily block the pressure-sensitive elements. Therefore, the flow measured by the flow meter was significantly distorted.

In this study, the downstream side of the test box was designed as a rectangular sharp-crested weir, which was used to monitor the water flow. There were two pore pressure meters (Fig. 5) embedded in the position of the dam heel to measure the water depth in front of the weir. The flux process of dam break flow could be inverted from the water depth in front of the weir.

#### 2.1.4 Data Acquisition

The data acquisition of the centrifugal model test system was composed of an Isolated Measurement Pod (IMP) data acquisition module and an Industrial Personal Computer (IPC). Eight IMP collection modules were used to provide 80 data acquisition channels, and the real-time control, collection, and storage of monitoring data were realized through the computer. In addition, through cameras placed on the test-box top, the gradual failure process of the barrier dam and the development under the break-flow effect could be monitored in a timely manner. The IPC and the cameras are shown in Fig. 6.

### 2.2 Scaling Issues

Newton's gravity is equivalent to the inertial force; thus, the physical effect of the gravity of a prototype is consistent with the centrifugal force in the centrifugal field. Centrifugal model tests mainly simulate gravity by centrifugal force. In this way, the gravity of the model structure is increased to the prototype state, and the stress states of the model and the prototype are consistent. In addition, the inherent property of soil material is mainly related to its micro-electromagnetic force, and the electromagnetic force is much less than its gravity or centrifugal force. Therefore, in the centrifugal field, properties of soil material will hardly ever change (Chen *et al*., 2012; Wang *et al*., 2011). In addition to the soil properties, model scale issue of several parameters needs further discussion. In particular, subscript p and m in the following formula represent prototypes and models respectively.

#### 2.2.1 Hydrodynamic Condition

Assuming that the flow is a constant flow in the process of

(a) (b)

Fig. 6. Data Acquisition System: (a) The Industrial Personal Computer, (b) Cameras Placed on the Model Box

barrier-dam overtopping, according to the Chezy formula, the flux is as follows:

$$v = \left(\frac{8g}{f}\right)^{\frac{1}{2}} R^{\frac{1}{2}} J^{\frac{1}{2}} \tag{1}$$

where $f$ is the friction coefficient, $R$ is the hydraulic radius, and $J$ denotes hydraulic gradient. According to Eq. (1), the velocity of water flow is independent of acceleration. In addition to the kinematic similarity, centrifuge model tests also must align with dynamic similarity. Parameters that can describe dynamic similarity generally include the Reynolds number, Froude number, Maher number, Euler number, etc. In general, dynamic similarity only must retain the Reynolds number and Froude number of the model as being identical to that of the prototype. The Reynolds number can be calculated by the following equation:

$$\mathrm{Re} = \frac{v\rho d}{\mu} \tag{2}$$

where $\mu$ denotes the dynamic viscosity coefficient. The general flow velocity is large in the process of barrier dam breaching, and the viscous force of fluid is not the controlling factor in this process. It is therefore necessary to conform to the Froude number of the model and the prototype agreement. The Froude number is as follows:

$$Fr = \frac{v}{\sqrt{gh}} \tag{3}$$

In the centrifuge model test, the centrifugal acceleration is $N$ times the acceleration of gravity (This means that when $N$ = 1, the centrifugal acceleration is 9.8 m/s$^2$.), and the water depth is 1/$N$ times the prototype. Thus, from the equation above, the Froude numbers of models and prototypes are consistent. That is, the centrifugal model test of overtopping aligns with the dynamic similarity.

### 2.2.2 Breach Discharge Calculation

The hydraulic literature provides explicit rules for the calculation of weir flows under normal gravity conditions (Padulano *et al*., 2016). However, references to the applicability of these methods in the centrifuge field are infrequent. Therefore, to obtain an accurate breach flow in the test, the calculation method of the rectangular sharp-crested weir flow in the centrifugal field is deduced.

As shown in Fig. 7, a section of flow layer of an infinitesimal thickness of $dh$ was obtained as the object of study at the depth of $h$ in the overflow section. The flow velocity of the infinitesimal flow layer was determined to be converted from potential energy, and the internal energy loss due to the fluid viscosity was neglected. Under the condition of $N$g centrifugal acceleration, it could be obtained from energy conservation that:

$$mNgh = \frac{mv^2}{2} \tag{4}$$

where $m$ is the mass of the infinitesimal flow layer, and $v$ is the flow layer velocity. Therefore, when ignoring the near velocity influence, the velocity in the flow layer is as follows:

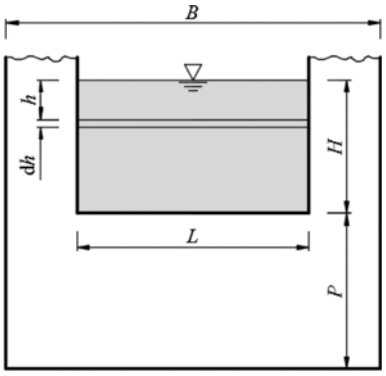


Fig. 7. Sketch of Rectangular Weir Flow Calculation

$$v_h = \sqrt{2Ngh} \tag{5}$$

Therefore, the flux of the flow layer in an ideal situation is as follows:

$$dQ = \sqrt{2Ngh}dA = L\sqrt{2Ngh}dh \tag{6}$$

where $L$ is the width of the rectangular weir, and $A$ represents the section area of the flow cell. The local energy loss caused by transverse contraction of the rectangular wing wall at both sides of the rectangular weir is ignored, as is the water jet contraction of outflow. Thus, the actual flow is less than that of the ideal case. For that reason, Eq. (6) introduces the lateral contraction coefficient $\sigma_c$ and the flow coefficient $\sigma_f$ to correct the actual flow. The rectangular weir flow $Q$, as follows, can be obtained by integrating Eq. (6) over the weir overflow depth, $h$:

$$Q = \int_0^H \sigma_c \sigma_f L\sqrt{2Ngh}dh \tag{7}$$

Hence, the equation for calculating the flux of the rectangular sharp-crested weir can be obtained by integration as follows:

$$Q = \frac{2}{3}\sigma_c \sigma_f L\sqrt{2Ng}H^{\frac{3}{2}} \tag{8}$$

where $H$ is the water head before the weir without near velocity, $\sigma_c$ denotes the lateral contraction coefficient, and $\sigma_f$ represents the flux coefficient. These two coefficients can be calculated by the Berezinski formula as follows (Andrea *et al*., 2017):

$$\begin{cases} \sigma_f = 0.32 + 0.01\dfrac{3-\dfrac{P}{H}}{0.46+0.75\dfrac{P}{H}}, 0 < \dfrac{P}{H} < 3.0 \\ \sigma_f = 0.32, \dfrac{P}{H} \geq 3.0 \\ \sigma_c = 1 - \dfrac{0.19\left(1-\dfrac{L}{B}\right)}{\sqrt[3]{0.2+\dfrac{P}{H}}}\sqrt[4]{\dfrac{L}{B}} \end{cases} \tag{9}$$

where $P$ is the height of the rectangular weir, and $B$ represents the inside net width of the test box.

### 2.2.3 Time Scale

For the pore water flow in the model soil, when the flow velocity and distance are $v_m$ and $\Delta l_m$, respectively, the time required is as follows:

$$t_m = \frac{\Delta l_m}{v_m} = \frac{\Delta l_m \mu_m}{k_m \rho_m g i_m} \tag{10}$$

where,

$$\begin{cases} \Delta l_m = \dfrac{1}{N}\Delta l_p \\ \mu_m = \mu_p \\ k_m = N k_p \\ \rho_m = \rho_p \\ i_m = i_p \end{cases} \tag{11}$$

Equation (10) can be converted into the following:

$$t_m = \frac{\dfrac{\Delta l_p}{N}\mu_p}{N k_p \rho_p g i_p} = \frac{\Delta l_p}{N^2 v_m} = \frac{t_p}{N^2} \tag{12}$$

From the formula above, the model seepage time—such as the dissipation time of excess pore water pressure, and the consolidation time—is generally $1/N^2$ times that of the prototype. Moreover, the inertia time of the model is $1/N$ times that of the prototype, and the breach flow and expansion process do not involve the flow of pore water. Thus, it is more appropriate to adopt the inertial time scale relation $1/N$ when analyzing these processes and parameters. For $N$g centrifugal model tests, the scaling relations of the common physical quantities are shown in Table 1.

## 2.3. Model Design

### 2.3.1 Preparation of Model Dam Material

Dam breaching is the process of the interaction between the breach soil and water flow in terms of microcosmic mechanisms. Therefore, the shear stress in the interface of soil and water is the main factor affecting the development of the breach. Furthermore, erosion resistance of dam material and the breach flow state are the governing factors during the breaching model tests. Hence, for open channel uniform flow, there is:

$$F_\tau = G \sin\theta = GJ \tag{1}$$

where $F_\tau$ denotes the shear force, $G$ represents the gravity of water, and θ is the bottom inclination of the open channel. Suppose that χ is the wetted perimeter, then:

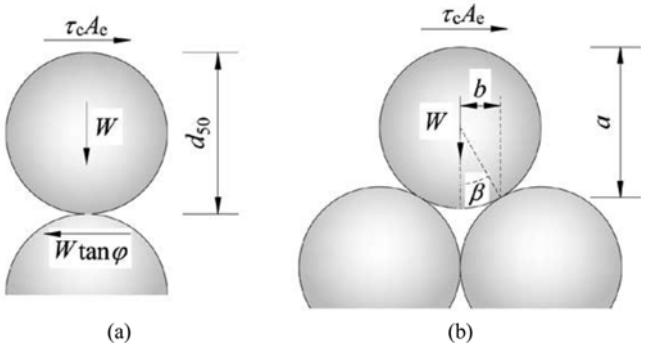


Fig. 8. Force Analysis of Cohesionless Particles: (a) Slip, (b) Rolling

$$\tau = \frac{GJ}{\chi l} = \rho_w N g R J \tag{2}$$

where $G$ is the density of water, $l$ represents the study length of the open channel, and $Ng$ denotes the centrifugal acceleration. For $R_m = R_p / N$ and $J_m = J_p$, it has the following

$$\tau_m = \tau_p \tag{3}$$

For dam material, the movement modes of cohesionless particles under the action of water erosion are slippage and rolling (Fig. 8). White (1940) suggested that the critical shear stress of particles slip is as follows:

$$\tau_c = \frac{W \tan\varphi}{A_e} \tag{4}$$

where $\varphi$ is the internal friction angle, $A_e$ represents the effective contact area between particles, and $W$ is the particle weight. For round particles:

$$\tau_c = \frac{2(\rho_s - \rho_w) N g \tan\varphi}{3\alpha} d_{50} \tag{5}$$

Here, $\alpha$ is the ratio of $A_e$ to the maximum cross-sectional area of particles, $d_{50}$ denotes the mean particle size, and $\rho_s$ is the soil density. The critical shear stress of particle rolling is as follows:

$$\tau_c = \frac{Wb}{A_e a} \tag{6}$$

For round particles:

$$\tau_c = \frac{2(\rho_s - \rho_w) N g \sin\beta}{3\alpha(1+\cos\beta)} d_{50} \tag{7}$$

Table 1. Similarity Criterion of Common Physical Quantity in Centrifugal Model Test

| Index | Acceleration | Length | Density | Mass | Time (inertia) | Time (seepage) |
|---|---|---|---|---|---|---|
| Similarity ratio | N | 1/$N$ | 1 | 1/$N^3$ | 1/$N$ | 1/ $N^2$ |
| Index | Force | Viscosity | Normal stress | Cohesion | Froude number | Permeability coefficient |
| Similarity ratio | 1/$N^2$ | 1 | 1 | 1 | 1 | N |

The definitions of parameters *a*, *b*, and β are shown in Fig. 8. From Eq. (7), the critical shear stress is proportional to the average particle size. Suppose $F_s = \frac{\tau}{\tau_c}$; then:

$$F_s = \frac{\tau}{\tau_c} = \frac{3\alpha(1+\cos\beta)\rho_w NgRJ}{2(\rho_s - \rho_w)Ng\sin\beta d_{50}} = \frac{3\alpha(1+\cos\beta)J}{2(G_s-1)\sin\beta}\cdot\frac{R}{d_{50}} \quad (8)$$

where $G_s$ is the specific gravity of soil particles. From Eq. (8), it can be shown that soil particles will erode if $F_s \geq 1$. During the model test, to ensure that the erosion rates of the model and prototype are consistent, the test must have $(F_s)_m = (F_s)_p$. Owing to $R_m = R_p / N$, to make the test process more accurate, for the cohesionless particles of the model material, the test must have the following:

$$(d_{50})_m = (d_{50})_p / N \quad (9)$$

For the cohesive particles, the governing factor of erosion is not the grain size, but its content. Thus, considering the wide gradation characteristics of the material of the barrier dam, the gradation curves of five boreholes of the Tangjiashan landslide dam were referenced during the preparation of the model dam material (Liu *et al*., 2010), as shown in Fig. 9.

After grain size averaging, the mean particle size $(d_{50})_m$ of the test material is controlled as $(d_{50})_p/N$, and the content of the cohesive particles remains unchanged. Then, $(d_{100})_m$ can be acquired. According to the average gradation curve of the Tangjiashan landslide dam, an equivalent alternate method is adopted to replace the particle size larger than $(d_{100})_m$ with that of 0.075~$(d_{100})_m$ mm. In this experiment, the centrifugal acceleration was set to 30 g ($N = 30$), and the gradation curve of the model dam material is shown in Fig. 10.

According to the model dam gradation curve, the content of each particle group, by weight, could be determined. After sifting, weighing, and stirring, the model dam material was prepared. Each particle group is shown in Fig. 11.

In addition to the particle size contraction scale, there were $\rho_m = \rho_p$ in the centrifuge model tests. It was therefore also necessary to ensure that the model and prototype dam material had the same dry density, whose value was 1.59 g/cm$^3$.

In dam break tests, erodibility of the soil used has a great influence on the erosion process of the model dam. Normally, the erosion resistance of soil is characterized by incipient velocity, which was measured through flume tests. Besides, shear strength of the soil is also an important index reflecting soil erosion resistance, which was also measured by three axis compression tests. The basic parameters of the model dam material are shown in Table 2.

In particular, this experiment did not fully simulate the discharge process of the Tangjiashan barrier dam. This is because, by simulating only the dam height, the centrifuge acceleration would have to been adjusted to 500 g, which would far exceed the rated operating value of the equipment. Therefore, in this experiment, only the dam material parameters were adjusted according to the Tangjiashan landslide dam for the model construction.

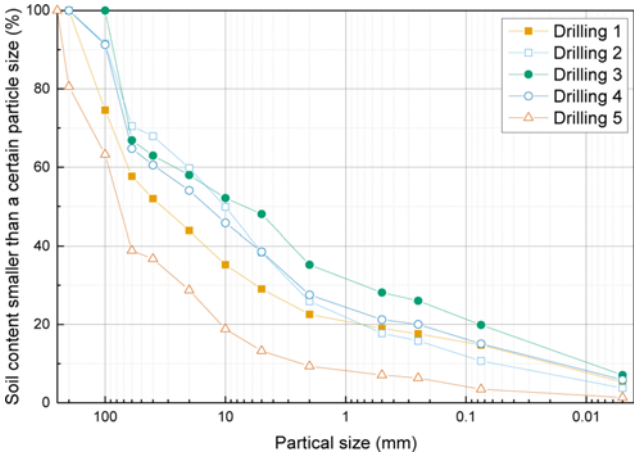


Fig. 9. Gradation Curves of Tangjiashan Barrier Dam

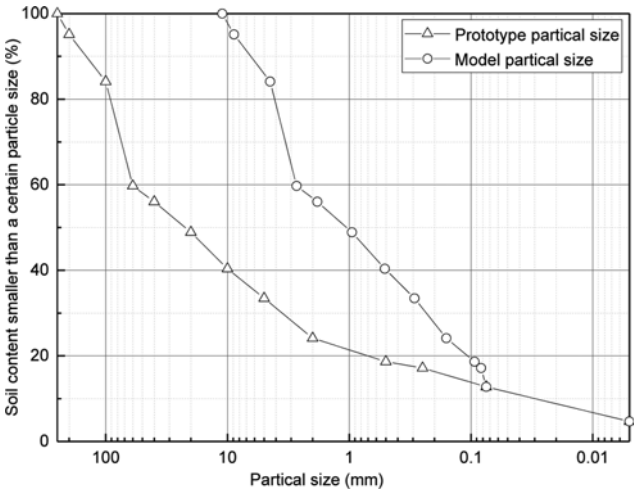


Fig. 10. Gradation Curves of Model Dam and the Average Gradation of Tangjiashan Barrier Dam

### 2.3.2 Construction of Model Dam

It is known that the angle of the dam downstream slope has an important influence on the development of a breach and the break flow. Thus, under the premise that the effective space inside the box is fully used, the design of the model dam should meet the requirement of the slope angle of the barrier dam being adequately small, similar to a real situation. According to the internal dimensions of the test box, the slope ratio of the dam downstream was 1:3.5, the dam crest width was 20 cm, the dam height was 20 cm, and the upstream slope ratio was 2:1. The bottom of the test box was a clay layer with a thickness of 15 cm. On the downstream of the model dam, the tail water, which was 5 cm in depth, was used for the weir flow calculation.

To study the breach development process, an inverted trapezoid groove (Fig. 12) was excavated from the middle of the dam crest as an initial breach to avoid the break water flow across the

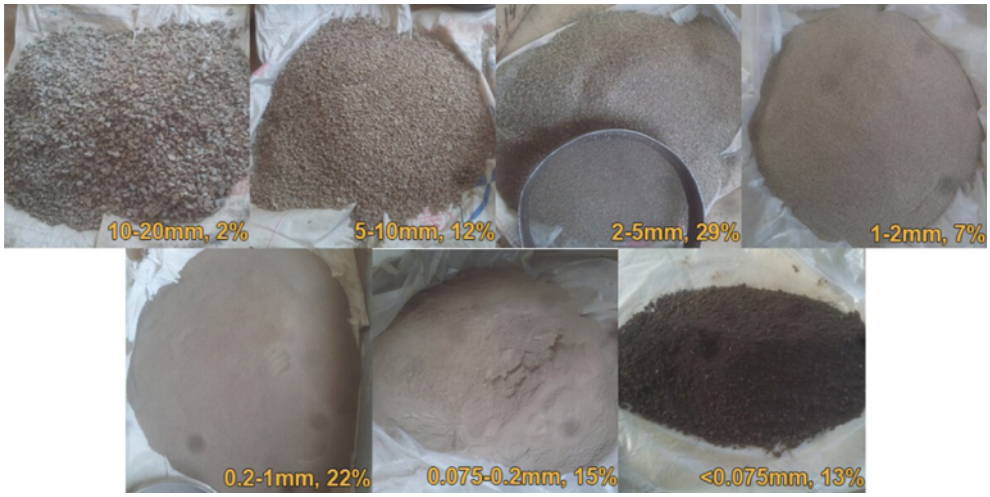


Fig. 11. Soil Samples and Contents of Each Particle Group

Table 2. Parameters of Model Dam Material

| Index | Median diameter ($d_{50}$, mm) | Restricted particle diameter ($d_{60}$, mm) | Dry density ($\rho_d$, g/cm$^3$) | Porosity ($n$, 1) |
|---|---|---|---|---|
| Value | 1.1 | 2.7 | 1.59 | 0.4 |
| Index | Permeability coefficient ($k$, cm/s) | Incipient velocity ($v_i$, m/s) | Internal friction angle ($\varphi_u$, °) | Cohesion ($c_u$, kPa) |
| Value | $1.0\times10^{-3}$ | 0.267 | 22 | 25 |

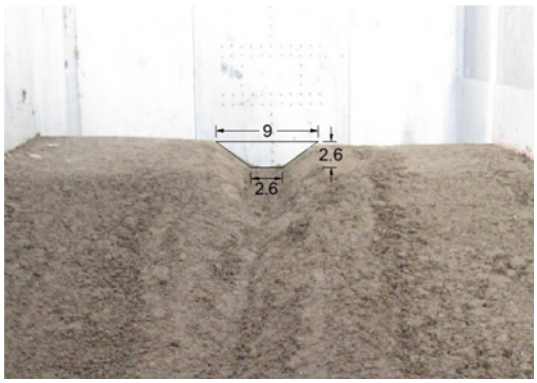


Fig. 12. Initial Breach of Model Dam (Unit: cm)

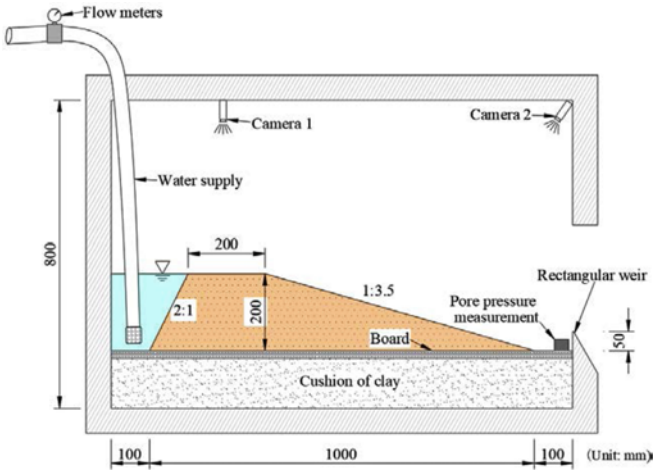


Fig. 13. Overall Layout inside the Test Box

whole dam crest. The size of the groove was 9.0 cm in the top width, 2.6 cm in the bottom width, and 2.6 cm in depth.

The model dam was constructed according to the dry density of 1.59 g/cm$^3$. The water supply pipe was an inlet on the bottom of the dam upstream. To prevent the water supply from directly eroding on the upstream slope, the pipe outlet was wrapped with gauze. The internal overall layout of the test box is shown in Fig. 13.

According to the design proposal, model dam was constructed in the box, as shown in Fig. 14. Then, put the model box in the basket of centrifuge by use of gantry crane. The basket of the centrifuge is shown in Fig. 15.

## 3. Experimental Results

Dam break is a complex process of soil and water interaction, and the dam break process has very poor repeatability. During this process, there are many accidental factors that affect the development of dam break. In order to verify the repeatability and the generality of barrier dam failure behaviors, two groups of dam break tests, named as Test 1# and Test 2#, with same working conditions were conducted respectively.

The breaching flow supply mainly depends on the upstream reservoir inflow during the dam break. Thus, during the process of dam failure, there has little change in water supply in general. According to the average inflow of Tangjiashan barrier lake and similar scale, the water supply flow in the tests was set to 0.02 m$^3$/s. During the model test, model dam development continued

Fig. 14. Profile of the Model Dam

Fig. 15. The Basket of the Centrifuge and the Test Box

to be observed until no deformation appeared in the breach and downstream slope under this scouring flow condition. Then, the water supply was stopped accordingly.

### 3.1 Process of Landslide Dam Failure

Through two sets of centrifugal model tests of barrier dam overtopping, the dam break image could be obtained, as shown in Figs. 16 and 17. Accordingly, the whole dam break process could be divided into five stages.

#### 3.1.1 Erosion on Downstream Slope

Dam-break water flows by the initial breach, and first erodes the downstream slope. In this stage, initial notching forms on account of the effect of overtopping flow at the downstream slope. There are small scarps in the notching, while headcut erosion does not exist. The erosion process is dominated by surface erosion. In this stage, flow in notching is low, and the breach development is relatively slow, as shown in Figs. 16(a) and 17(a).

#### 3.1.2 Notch Cutting

At this stage, the dam break water flow gradually increases. Horizontal expansion and vertical cutting occur in the notching on the downstream slope, and the speed of vertical cutting is faster than the width expansion. Development of a breach is dominated by vertical cutting, as shown in Figs. 16(b) and 17(b).

#### 3.1.3 Notch Wall Scouring

Owing to the rapid breach cutting, the water head continuously increases, leading to the increase of breach flow and dam erosion. Vertical cutting of the breach was nearly completed in the previous stage; hence, the breach flow mainly acts on both sidewalls of the breach in this stage, resulting in the fast expansion of the breach width. The breach horizontal expansion is predominantly in the form of continuous erosion in this stage,

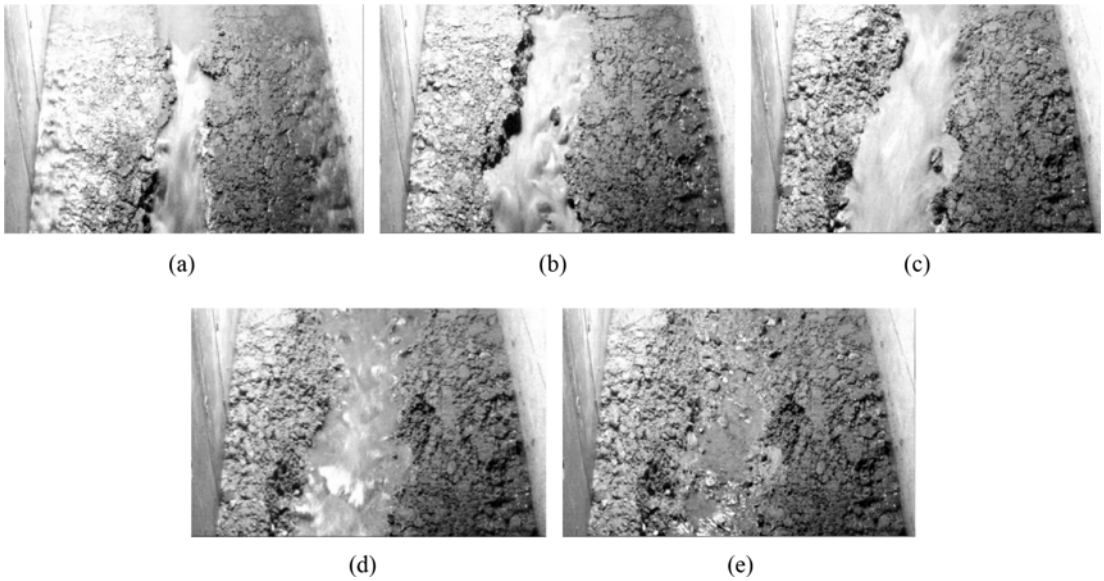


Fig. 16. The First Set of Dam Break Test: (a) 6.5 min after Overtopping, (b) 10 min after Overtopping, (c) 24 min after Overtopping, (d) 35 min after Overtopping, (e) 58 min after Overtopping

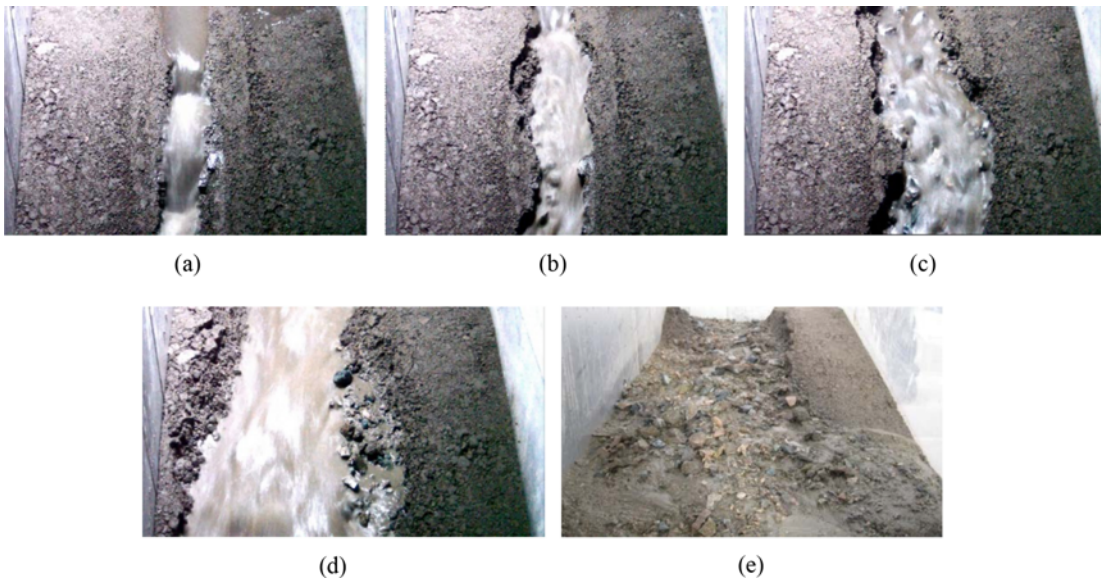


Fig. 17. The Second Set of Dam Break Test: (a) 6.5 min after Overtopping, (b) 10 min after Overtopping, (c) 24 min after Overtopping, (d) 35 min after Overtopping, (e) 58 min after Overtopping

as shown in Figs. 16(c) and 17(c).

#### 3.1.4 Dam Breach Collapse

The breach continues to expand in the width-wise direction. Because the break water does not flow across the whole section of the breach, the sidewalls are eroded mainly in the middle and lower parts, which will inevitably cause an angle increase in the breach sidewalls. When the angle increases to a certain extent, soil on both sides of the breach will collapse. In this stage, the breach width alternately expands in the forms of continual erosion and collapse on the sidewalls. Owing to the new expansion form, which is the sidewall collapse in this stage, the speed of the width-wise expansion is much faster than that of the previous stage. It is depicted in Figs. 16(d) and 17(d).

#### 3.1.5 Downstream Slope Coarsening

In this stage, breach width expansion and vertical cutting obviously slows, and the water head continually decreases along with the decrease of breach flow. Owing to the wide grading of barrier dam materials, the small soil particles are taken away by the break flow, and large particles, such as gravel and boulders, remain on the downstream slope because they do not meet the critical starting condition, which results in coarsening of the downstream slope. As the break flow decreases, small particles are almost fully removed, and breach development gradually stops. The remaining dam is shown in Figs. 16(e) and 17(e).

According to the five stages of the barrier dam break process, the failure mode of barrier dam overtopping is similar to that of the homogeneous sand dam; both are surface erosion. The barrier dam overtopping failure process mainly consists of continuous notch cutting and width expansion caused by the dam break flow, as well as intermittent width expansion caused by the breach slope collapse. Unlike the homogeneous sand dam, the barrier dam breach is rapidly cut at the initial stage of overtopping.

However, owing to the existence of larger particles in the barrier dam, such as gravel and boulders, the longitudinal development of the breach is prevented. Therefore, the breach cutting ceases early and continues to develop in the transverse direction. Through the residual breach (Fig. 17(e)), it is obvious that breach cut of the barrier dam is shallow and considerably smaller than the width expansion distance. Moreover, coarsening can be observed on the downstream after the dam break.

### 3.2. Discharge Process Analysis

Through calculation of the monitoring data from the rectangular weir, the curve of breach flow is acquired. In this experiment, the downstream water level was low. On account of the shielding of the upper part of the test box, the wind field in the centrifuge room while running had minimal influence on the whole test process. The weir water head in the prototype scale could be acquired according to the centrifugal acceleration, and it is conformed to the specification for the rectangular weir flow calculation. According to the data of two sets of the barrier-dam break centrifugal model tests, breach flow curves could be calculated, as shown in Fig. 18. In the figure, the elapsed time starts when the model dam upstream begins to store water. The elapsed time and breach flow are analyzed in the prototype scale according to the centrifugal acceleration. The elapsed time is the inertial time, whose scale relation is $1/N$.

Figure 18 shows that the breach flow of the two sets of tests is low during a relatively long time period at the beginning of the dam break; the value is approximately 1.5 $m^3/s$. At approximately 41 min after the dam failure, discharge of the breach flow sharply increases with an acceleration of approximately 0.161 $m^3/s^2$, and the breach flow in the first sets of tests is approximately 1 min later than that of the second sets. Through the failure

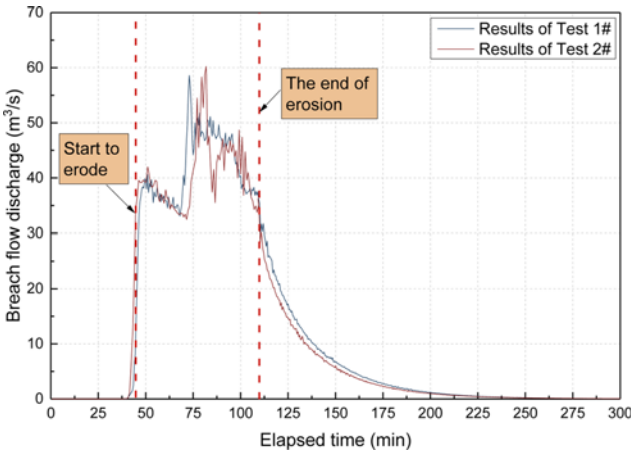


Fig. 18. Curves of Breach Flow in the Two Sets of Tests

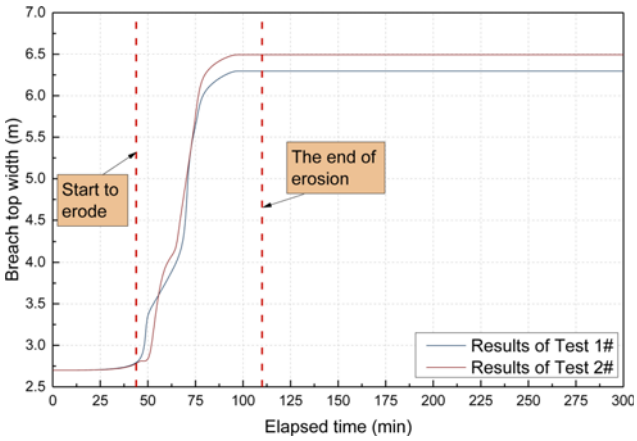


Fig. 19. The Development of Breach Top Width

mechanism previously analyzed, the breach development is dominated by notch cutting at this stage. Thus, when the dam erosion begins, the breach bottom elevation rapidly decreases, and the water head increases sharply along with the increase of breach flow.

Approximately 51 min later, the breach flow in the two sets of experiments reached 40.6 $m^3/s$ and decreased in the same degree from that point. This is because the breach bottom cutting to the final elevation was under the effect of the flow discharge; then, the water head gradually decreased, resulting in the decrease of flow after the peak flow. Thereafter, the breach flow increased again to 60.2 $m^3/s$, and the flood peak time of the two sets of tests was 73 and 82 min, respectively. In this stage, the breach flow had the strongest erosion capability, and the breach development was dominated by width expansion. As the breach soil on both sides flowed away, the breach width continually expanded, and the breach flow fluctuated during this time. Subsequently, the breach flow decreased and the scour process gradually disappeared. The breach was fully developed until this point. Meanwhile, the armor layer appeared on the downstream slope, and the whole dam break process concluded.

### 3.3 Analysis of Breach Top Width Development Process

The breach top width development process was documented by a dam break video. The elapsed time was calculated by the scale relation of inertial time, whose value was 1/*N*. The breach top width development is shown in Fig. 19. In this figure, the development process corresponds to the breach flow discharge process. At the beginning, the pace of the breach horizontal expansion is slow. Meanwhile, the development speed of the breach top width increases significantly at approximately 41 min after overtopping, and the value was approximately 10.5 m/h. In this stage, the breach flow also sharply increased.

Approximately 51 min later, the expansion speed of the breach top width began to slow, and the breach flow became progressively less along with the decrease of dam erosion in this stage. At approximately 70 min later, breach flow increased once again, and the breach width expansion sped up accordingly. Approximately 89 min later, the breach top width expansion gradually slowed and marked the cessation of dam erosion. The remaining breach top widths were 6.30 and 6.50 m, respectively, through the two sets of model tests. These results indicated that the development of the breach width extended through the whole dam break process. In the early stages, breach width expansion was slower than the notch cutting. As the breach flow decreased, the breach was cut into the final elevation of the bottom in a very short time period. From that point, the breach development was dominated by width expansion.

## 4. Conclusions

In this study, centrifugal model tests of dam failure due to overtopping were conducted based on the gradation curves of the Tangjiashan barrier dam. We thereby derived a calculation method of rectangular weir flow in the centrifugal field. Based on centrifuge model tests of barrier dam overtopping, the experimental data and videos were analyzed, and the conclusions under these experimental conditions are outlined below:

1. A centrifuge model test system of a dam break was established, and a series of physical simulations of barrier dam overtopping was performed based on the system. The applicability of the measuring weir in breach flow measurement in the centrifugal field was proved.
2. The barrier dam overtopping process is divided into five stages: 1) erosion on the downstream slope; 2) notch cutting; 3) notches wall scouring; 4) dam breach collapse; and 5) downstream slope coarsening. The first four stages of barrier dam overtopping are similar to those of the homogeneous earth dam. However, the notch cutting of the barrier dam ceases at an earlier time and is basically completed in the first two stages, whereas the breach horizontal expansion starts at the beginning of the process and continues throughout it. The coarsening on the downstream slope in the fifth stage is relatively rare during a homogeneous earth dam break. Thus, downstream slope coarsening is the manifest characteristic of the barrier dam owing to wide grading.

3. In the latter period of a barrier dam break, the armor layer appears on the downstream slope. Large particles accumulate on the downstream slope and prevent further development of the breach. Along with the barrier lake water level and velocity decrease, the breach development slows down. Therefore, in practical engineering, the bottom part of barrier dam, which consists of earth and stone material with wide grading, would survive after dam breaching. Compared with barrier dam, homogeneous earth dam has a larger remaining breach, higher peak flow and more serious consequences after dam breaching under the same conditions.
4. In risk assessment and flood calculation of a dam break, owning to the situation of entire dam failure is relatively rare for a barrier dam, compared with entire dam-break, the condition of partial dam break must be fully considered. While, for a homogeneous earth dam, condition of total dam break or even breach cut down to the dam foundation, needs to be thoroughly calculated and analyzed.
5. In derivation of a mathematical model for barrier dam failure, coarsening on the downstream slope which have significant impact on dam failure process should be taken into account. Besides, there has been recent analytical solutions looking at flow of water and air in the porous media and deformation of the unsaturated soil (Ho *et al*., 2015; Ho *et al*., 2016), and the wetting deformation of unsaturated zone considering consolidation in the dam is a key point of barrier dam break calculation.
6. In design of a homogeneous dam, grading of dam materials can be widened on a reasonable basis; for instances, coefficient of uniformity ($C_u$), and coefficient of curvature ($C_c$) in grading curve should be fully considered. And a small amount of large particles can be added to dam materials, which can effectively prevent notch cutting from developing too fast and further reduce the peak flow in breach.

In particular, the selection of model dam materials, in this experiment, is based on the parameters of Tangjiashan landslide dam material. However, different dam materials parameters have different effects on dam failure process. The future researches should focus on the influence of different material parameters and hydraulic conditions on dam break process.

## Acknowledgements

The authors gratefully acknowledge the financial support from the National Natural Science Foundation of China under Grant No. 51709025, the National Science and Technology Support Program of China under Grant No. 2015BAK09B01, and the Chongqing Science and Technology Commission of China under Grant No. cstc2018jcyjAX0084, respectively.

## References

Becker, J. S., Johnson, D. M., and Paton D. (2007). "Response to landslide dam failure emergencies: Issues resulting from the October 1999 Mount Adams landslide and dam-break flood in the Poerua River, Westland, New Zealand." *Natural Hazards Review*, Vol. 2, No. 8, pp. 35-42, DOI: 10.1590/S1413-95962004000200002.

Bruijn, K. D., Klijn, F., Ölfert, A., Penningrowsell, E., Simm, J., and Wallis, M. (2009). *Flood risk assessment and flood risk management*, *An introduction and guidance based on experiences and findings of FLOODsite (an EU-funded Integrated Project)*, Hydraulic Engineering Reports, Deltares.

Chen, S., Xu, G., Zhong, Q., and Gu, X. (2012). "Development and application of centrifugal model test system for break of earth-rock dams." *Journal of Hydraulic Engineering,* Vol. 43, No. 2, pp. 241-245, DOI: 10.13243/j.cnki.slxb.2012.02.006.

Corns, C. F. (2010). "Status report on the national dam safety program." *Safety of Small Dams*, ASCE, pp. 4-7.

Davies, T. R. (2002). "Landslide-dambreak floods at Franz Josef Glacier township, Westland, New Zealand: A risk assessment." *Journal of Hydrology (New Zealand)*, Vol. 41, No. 1, pp. 1-17.

Davies, T. R., Manville, V., Kunz, M., and Donadini, L. (2007). "Modeling landslide dambreak flood magnitudes: Case study." *Journal of Hydraulic Engineering*, Vol. 133, No. 7, pp. 713-720, DOI: 10.1061/(asce)0733-9429(2007)133:7(713).

Gregoretti, C., Maltauro, A., and Lanzoni, S. (2010). "Laboratory experiments on the failure of coarse homogeneous sediment natural dams on a sloping bed." *Journal of Hydraulic Engineering,* Vol. 136, No. 11, pp. 868-879, DOI: 10.1061/(ASCE)HY.1943-7900.0000259.

Ho, L. and Fatahi, B. (2016). "One-dimensional consolidation analysis of unsaturated soils subjected to time-dependent loading." *International Journal of Geomechanics*, Vol. 16, No. 2, 4015052, DOI: 10.1061/(ASCE)GM.1943-5622.0000504.

Ho, L., Fatahi, B., and Khabbaz, H. (2015). "A closed form analytical solution for two-dimensional plane strain consolidation of unsaturated soil stratum." *International Journal for Numerical and Analytical Methods in Geomechanics*, Vol. 39, No. 15, 1665-1692, DOI: 10.1002/nag.2369.

Jiang, H. (2007). "Study on process of barrier dam break and the flow change." *Technology of Soil and Water Conservation*, pp. 24-26.

Kuang, S. (1993). "Formation mechanisms and prediction models of debris flow due to natural dam failures." *Journal of Sediment Research*, No. 4, pp. 42-57.

Li, Y. and Li, J. (2009). "Review on experimental study on dam-break." *Advances in Water Science*, Vol. 20, No. 2, pp. 304-310, DOI: 10.1002/9780470686812.ch1.

Liu, N., Chen, Z., Zhang, J., Lin, W., Chen, W., and Xu, W. (2010). "Draining the tangjiashan barrier lake." *Journal of Hydraulic Engineering*, Vol. 136, No. 11, pp. 914-923, DOI: 10.1061/(ASCE)HY.1943-7900.0000241.

Lobovsky, L., Botia-Vera, E., Castellana, F., Mas-Soler, J., and Souto-Iglesias, A. (2013). "Experimental investigation of dynamic pressure loads during dam break." *Journal of Fluids and Structures*, Vol. 48, pp. 407-434, DOI: 10.1016/j.jfluidstructs.2014.03.009.

Maranzoni, A., Marco, P., and Massimo, T. (2017). "Experimental and numerical analysis of side weir flows in a converging channel." *Journal of Hydraulic Engineering*, Vol. 143, No. 7, 04017009, DOI: 10.1061/(ASCE)HY.1943-7900.0001296.

Mizuyama, T., Tabata, S., Mori, T., Watanabe, F., and Inoue, K. (2008). "The dam break and prevention of barrier dam." *Water Resources and Hydropower Engineering*, Vol. 39, No. 7, pp. 97-99, DOI: 10.3969/j.issn.1000-0860.2008.07.026.

Morris, M. W. (2000). "CADAM: Concerted action on dam break modelling." *HR Wallingford Limited.*

Morris, M. W. and Hassan, M. (2005). "IMPACT: Investigation of extreme flood processes and uncertainty - A European research project." *Proceedings of the 40th Defra Flood and Coastal Management Conference,* University of York, York, UK.

Padulano, R. and Giudice, G. D. (2016). "Transitional and weir flow in a vented drop shaft with a sharp-edged intake." *Journal of Irrigation & Drainage Engineering*, Vol. 142, No. 5, 6016002, DOI: 10.1080/23249676.2015.1026417.

Schuster, R. L. and Costa, J. E. (1986). "A perspective on landslide dams." *In Landslide Dams: Processes, Risk, and Mitigation*, *Proceeding of a Session in Conjunction with the ASCE Convention*, Seattle, WA, USA.

Wan, C. F. and Fell, R. (2004). "Investigation of rate of erosion of soils in embankment dams." *Journal of Geotechnical and Geoenvironmental Engineering*, Vol. 130, No. 4, pp. 373-380, DOI: 10.1061/(ASCE)1090-0241(2004)130:4(373).

Wang, Q., Chen, Z., Sui, H., Hou, Y., and Liang, J. (2011). "Modelling seepage flow velocity in centrifuge models." *Chinese Journal of Geotechnical Engineering*, No. 8, pp. 1235-1239.

Wang, X. and Liang, Z. (2008). "Experimental study on barrier dam break." *Technology of Soil and Water Conservation*, pp. 8-9.

Yan, Z., Wei, Y., and Cai, H. (2009). "Formation mechanism and stability analysis of barrier dam." *The Chinese Journal of Geological Hazard and Control*, Vol. 20, No. 4, pp. 55-59, DOI: 10.16031/j.cnki.issn.1003-8035.2009.04.021.